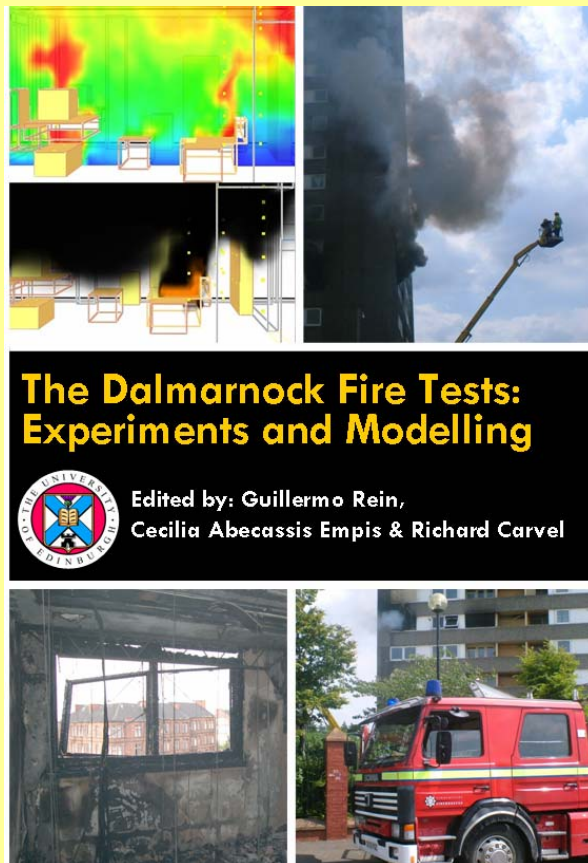


*This PDF file is an extract from:*

**The Dalmarnock Fire Tests: Experiments and Modelling**  
**Edited by G. Rein, C. Abecassis Empis and R. Carvel**



**Published by the School of Engineering and Electronics,  
University of Edinburgh, 2007.  
ISBN 978-0-9557497-0-4**

**The contents of the book and much of the other published output from  
the BRE Centre for Fire Safety Engineering can be downloaded for free  
from the Edinburgh Research Archive:**

**<http://www.era.lib.ed.ac.uk/handle/1842/1152>**

**Produced as part of the FIRESEAT symposium series:**

**<http://www.fireseat.org/>**

## 2. Experimental Layout and Description of the Building

*By Pedro Reszka, Cecilia Abecassis Empis, Hubert Biteau, Adam Cowlard, Thomas Steinhaus, Ian Fletcher, Andres Fuentes, Martin Gillie & Stephen Welch*

### Introduction

This chapter describes the experimental set-up of Dalmarnock Fire Tests One and Two. While Test One was planned to allow a fire to develop freely to post-flashover conditions, Test Two was designed to allow for ventilation management. A detailed account of the building layout, the set-up of the different experiments and measurements carried out during the full-scale tests is given, together with the specifics of the instrumentation installed in the building. A description of the fuel load and the ventilation conditions during both tests is also presented. Due to the large amount of data presented, the chapter is organised so that the most relevant information is shown in the main body of the text, and additional detail, such as the instrument coordinates, is appended in an annex at the end of the chapter.

### Description of the building

The experiments were carried out in a council estate in Dalmarnock (Glasgow). The structure was built in 1964 as a 23-storey residential tower comprising mostly of cast in-situ reinforced concrete. There were six flats per storey, three either side of an access corridor which also lead to two stairwells and elevator shafts. The two main experiments were held in identical apartments, located on different floors of the building but with identical layout and orientation, while the third, smaller test was held in one of the exit stairwells. Test Three had very simple instrumentation consisting mostly of smoke and gas detection and was mainly conducted by Xtralis personnel to test their early warning systems in a smoke management scenario. Hence, it is not further discussed.

Both flats used for the main tests were located on the north side of the building, facing westward. The apartment used in the first test was located on the 4<sup>th</sup> floor while the one used in the second test was located on the 2<sup>nd</sup> floor. The one storey gap between both tests prevented damaging the second apartment during the first experiment, protecting it from flames, smoke, heat and water seepage. The dwellings comprised a main flat corridor which led to two bedrooms, a bathroom and a living room which had an extra door leading to a small kitchen, as seen in Figure 1.

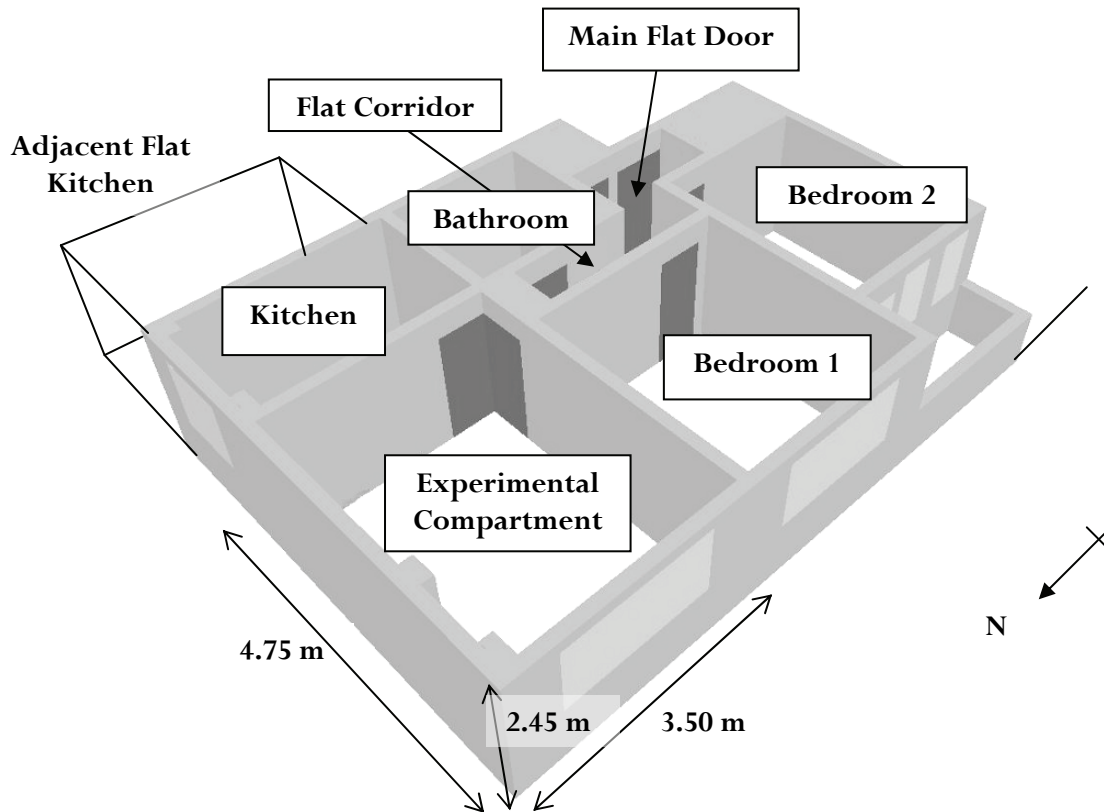


**Figure 1. Flat layout, viewed from the north-west. The adjacent flat kitchen where the data logging equipment was located is outlined.**

The experimental compartment was the living room: 2450 mm high and 3500 x 4750 mm with a 2350 mm wide by 1180 mm high set of windows (2 panes) on the west-facing wall, 1110 mm from the floor. The north and west walls of the experimental compartment were external, the west wall being load bearing. The north wall was largely non-load bearing, although it did contain two structural columns. Of the internal walls the south wall was structural and the second a light-weight partition wall dividing the fire compartment from the kitchen; this wall performed no structural function but prevented high temperatures developing on its outer side. The details of the support conditions of the slab above the fire compartment were, therefore, quite complex. However, the slab may be considered approximately as one-way spanning between fixed supports. Its nominal thickness was 150 mm and a survey using ground penetrating radar indicated that it contained mesh reinforcement near its lower surface over its entire area, with additional reinforcement near the top surface in the hogging regions adjacent to the supports.

## **Fuel loading**

All existing furnishings and finishes contained in the apartments were removed, except for the kitchen embedded furniture and the doors. In the 4<sup>th</sup> floor apartment, the wall separating the kitchen from the living room was removed and replaced by a lightweight

steel framing wall, which was fitted with various sensors, as will be discussed in the following sections. The kitchen door was removed with the original wall and was not replaced, as was the door from the corridor. Both experimental compartments were identically re-furnished. The general layout was such that most of the fuel was concentrated towards the back of the compartment, away from the window, with an even fuel loading throughout the rest of the compartment, as seen in Figures 2-4. This fuel configuration was intentionally very similar to the ISO room corner test (British Standards, 1993), allowing for entrainment during the fire to drive the flames against the flammable corner. This was intended to make the set up robust to environmental variables. The rest of the rooms were left empty, except for the instrumentation cables and rock wool insulation lain on the floors, used to cover the wires.



**Figure 2. Photographs of the Test One experimental compartment looking towards a) the NW corner and b) the NE heavily fuel-loaded corner. Fuel load and distribution was identical in both tests.**

The main fuel source in the experimental compartments was a two-seat polyurethane sofa, but they also contained two wooden office work desks with computers, each with its own foam-padded chair, three tall wooden bookcases, a short plastic cabinet, three small coffee tables and several paper and tall plastic lamps. The bookcases were fully-laden with books, video tapes, paper-filled cardboard files and several other plastic items, as was the small cabinet. The bookcase closest to the sofa also had two plastic containers holding thin cardboard boxes filled with polystyrene pellets. Beneath the central computer desk there were two plastic boxes filled with newspapers and magazines. Other minor living room/office items were included such that it appeared as if the compartment was “in use”. A plastic wastepaper bin filled with crumpled up newspaper and heptane was used as the ignition source. In the case of the uncontrolled burn, the amount of accelerant used was 500ml, while for the controlled burn the amount used was 300ml. The bin was placed between the sofa and a bookcase, underneath a blanket that was draped over the sofa arm. The floor of the room was covered with a carpet, under which ran all the instrumentation cabling. The fuel load density in the experimental compartment was estimated to be 32 kg/m<sup>2</sup> floor area, of wood equivalent.

## **Additional Demonstrations in Test One Non-Related to Fire Development**

Since Test One was expected to develop into a post-flashover fire, additional non-intrusive demonstrations were included in the Test One compartment. These were placed such that their behaviour and response to the fire could be monitored, while their presence remained passive to the fire development. These experiments included a steel truss assembly fixed to the ceiling across the compartment near the window, Fibre Reinforced Polymer (FRP) arrangements and a Perspex (PMMA) slab affixed to the partition wall shared with Bedroom 1.

The truss comprised of welded steel rods and angle sections, dimensioned to represent a truss system similar to those used in World Trade Centres 1 and 2, included purely for demonstration purposes and did not add any scientific value to the tests. The aim was to study its general qualitative behaviour in fire. The FRP arrangements comprised of three FRP plates and three FRP near-surface mounted rods applied to the lower surface of the west half of the compartment ceiling, in order to assess their fire resistance. One pair of FRP plates and rods was left unprotected, another protected with intumescent paint and the last pair was protected with gypsum board. While in Test One this arrangement was instrumented, a similar FRP arrangement in Test Two was left uninstrumented, for an additional study of qualitative behaviour in fire. The PMMA was introduced and rigged with sensors such that its exposure to the Test One fire could be used as part of an independent flame spread study.

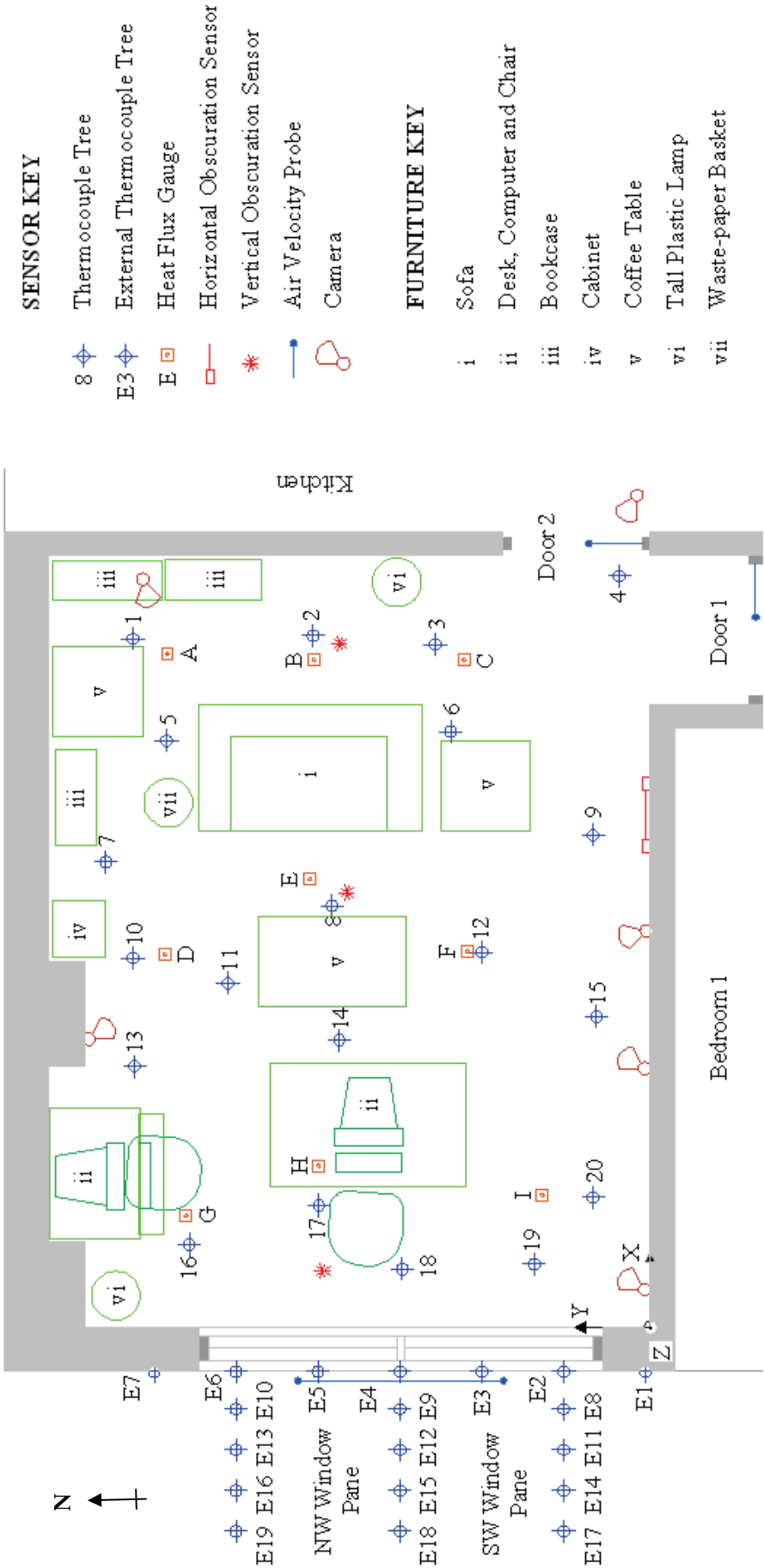


**Figure 3. Test One: plan view of experimental compartment showing the furniture layout and sensor locations. The global coordinate system origin for Test One is shown. This diagram is drawn to scale.**

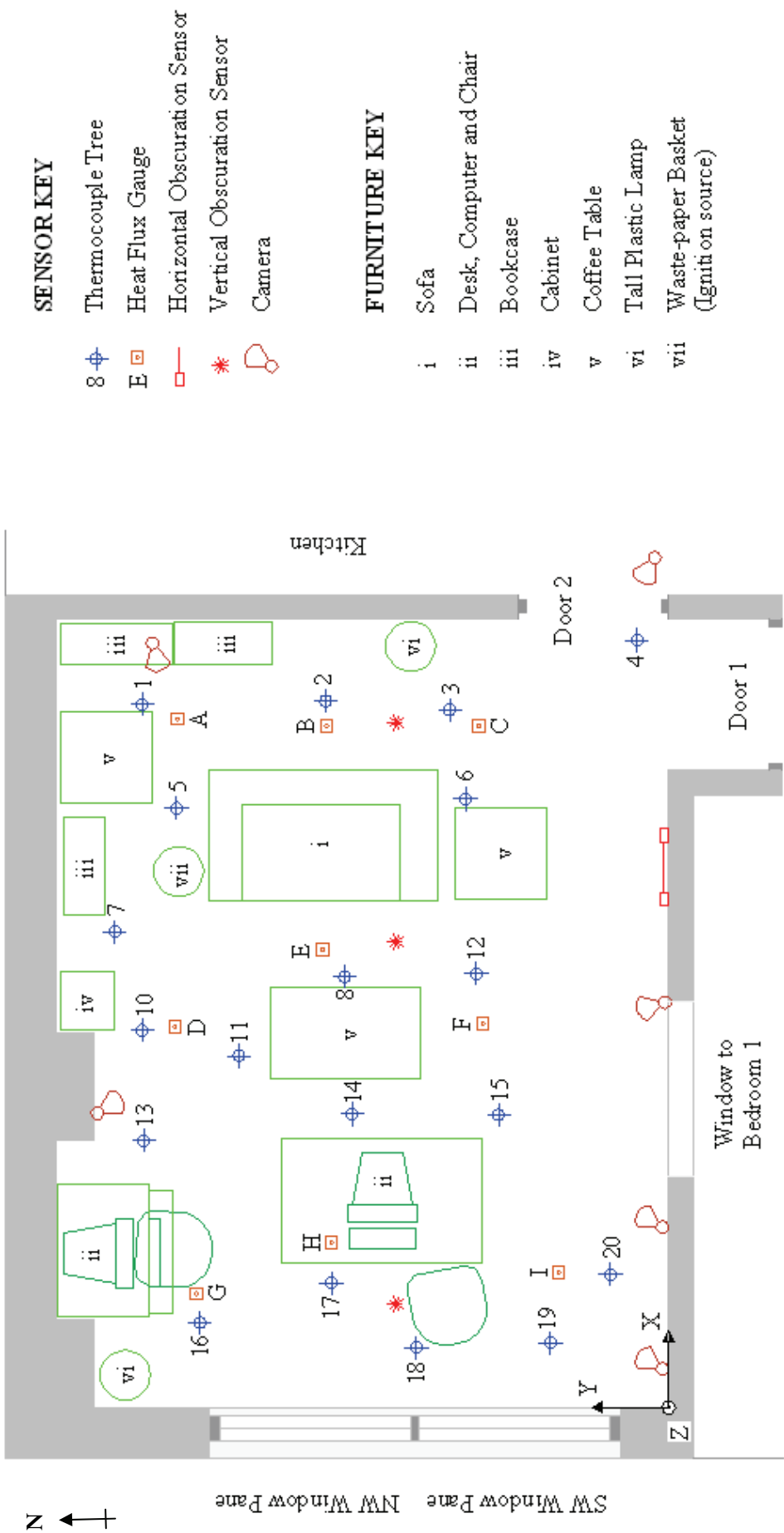


**Figure 4. Test Two: plan view of experimental compartment showing the furniture layout and sensor locations. The global coordinate system origin for Test Two is shown. This diagram is drawn to scale.**



## Ventilation

Ventilation parameters generally have a significant impact on fire development and fire behaviour. In the growth stage, fires are generally well-ventilated, but after the growing stage the fire can become ventilation-controlled. In ventilation-controlled fires combustion of the volatile species is incomplete, and the heat release rate will depend on the local equivalence ratio (Tewarson 1995).

In Test One, the initial conditions were such that the window in the main experimental compartment and that of Bedroom 1 were closed, those of Bedroom 2 were fully open and the kitchen window was left ajar. All doors throughout the flat were left fully open with the exception of the main front door which was left ajar and that of the bathroom compartment which remained sealed off throughout the experiment. These initial ventilation conditions are depicted in Figure 5 and subsequent changes in ventilation conditions are identified in “Major Events”, in Chapter 3.

Meteorological Office data for the test day (25<sup>th</sup> July 2006) shows that between the hours of 9am and 2pm, the humidity at the closest weather station was on average 57%, wind velocity and direction were significantly variable and the maximum and minimum ambient temperatures recorded that day were 27.1° and 12.7°C. Nevertheless, much more detailed records of local ambient temperature were recorded using the thermocouples used for the tests.

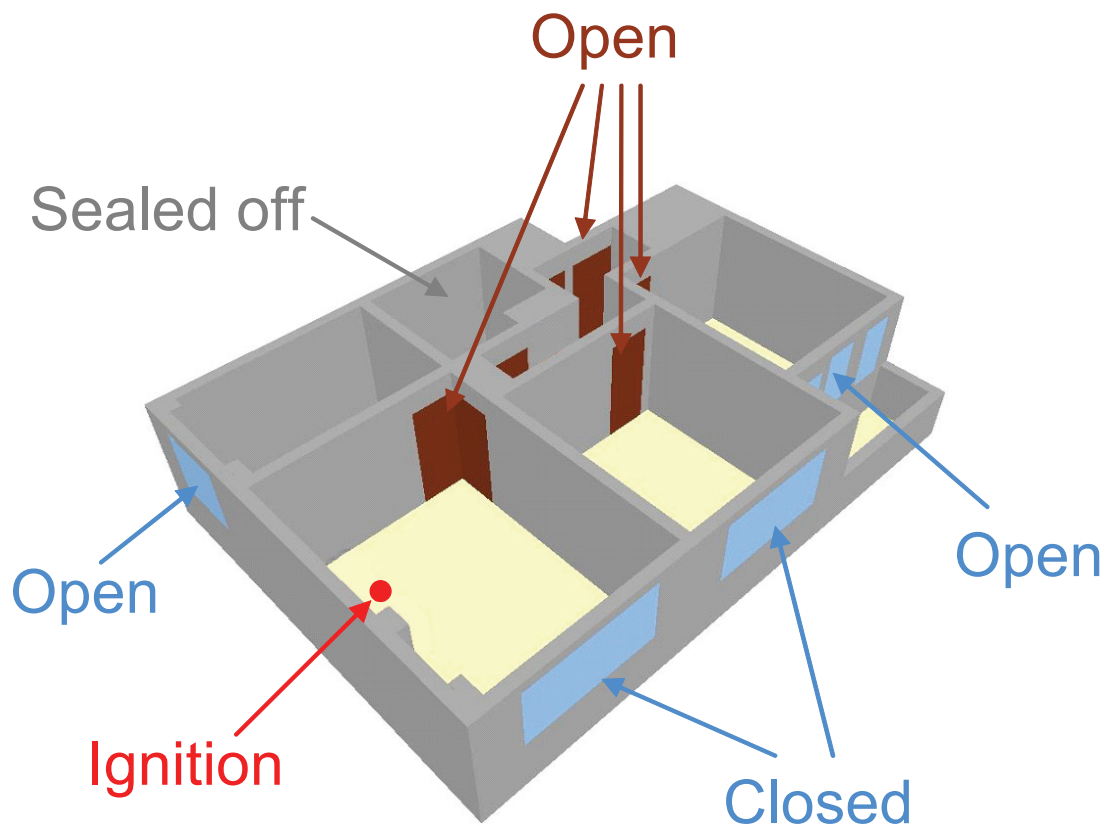


**Figure 5. Initial ventilation conditions for Test One.**



Ventilation conditions in Test Two were designed so that they could be altered throughout the experiment with the intention of influencing the growth of the fire. The main compartment window and its two doors were initially closed but could be opened or closed from outside the building via remote control. All other windows in the apartment and the two doors to the bedrooms were open. The front door to the apartment was initially closed but was also remotely controlled. There was also a large hole, approximately 1m wide, 0.5m high and 1m from floor level, in the wall separating the fire compartment from Bedroom 1. These initial ventilation conditions are indicated in Figure 6 while subsequent changes in ventilation conditions throughout the fire are detailed under “Major Events” in Chapter 4.

Meteorological Office data for the day of Test Two (26<sup>th</sup> July 2006) shows that, between the hours of 9am and 2pm, the humidity at the closest weather station was on average 69%. Wind velocities recorded were again considerably variable in velocity and direction and the maximum and minimum ambient temperatures recorded on the day of the test were 26.4° and 16.7°C. Nevertheless, once again, much more detailed records of local ambient temperature were recorded using the thermocouples installed for the tests.

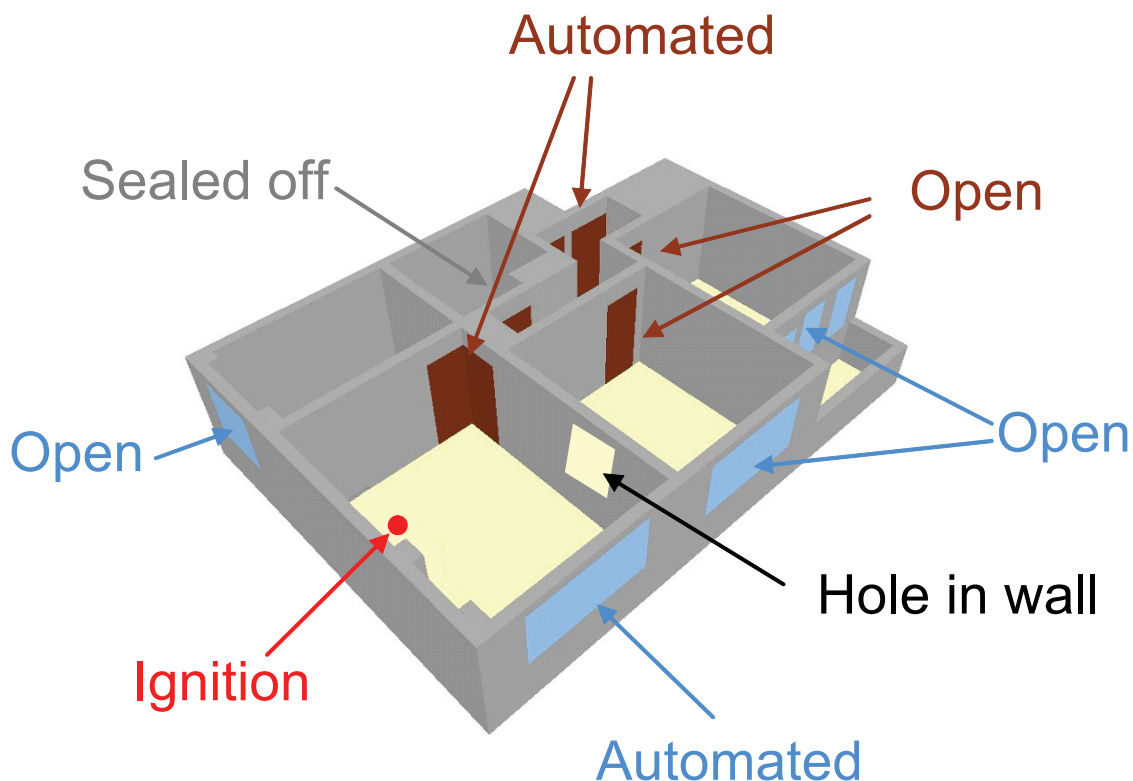


**Figure 6. Initial ventilation conditions for Test Two.**

## Coordinate system

Due to the large number of instruments placed in the apartments a global coordinate system was necessary for the setting up of the experiments and to avoid confusion during the data analysis process. Each test had an individual coordinate system. Thus, all instrument locations are given with respect to these coordinate systems. For the first test the origin was placed at the floor level on the southwest corner of the experimental compartment, on the 4<sup>th</sup> floor. The origin of the coordinate system for Test Two was also placed at the floor level on the southwest corner of the experimental compartment, but on the 2<sup>nd</sup> floor. Refer to Figures 3 and 4 for their exact location.

## Instrumentation

The experimental compartments were heavily instrumented, in order to obtain a high resolution of several different types of data associated to the development of both fires. The main types of instrumentation used throughout were thermocouples, heat flux gauges and laser smoke obscuration sensors, with bi-directional air velocity probes installed in Test One only. Additionally Test One included further instrumentation that provided data on a series of phenomena of interest to the ongoing research at the BRE Centre for Fire Safety Engineering. The following subsections detail both main compartment experiments and each individual demonstration, defining the aims of the particular trial and the instrumentation used. Due to the large number of sensors, their particular location is presented in the relevant tables and figures in the annex at the end of the chapter.

All the thermocouple wire used in this study was KX type (nickel-chromium), with fibreglass insulation with a 0.2 mm strand diameter and overall external dimensions of 2 x 3 mm, the average beaded end measuring about 1mm in diameter. The temperature rating for this type of insulation is of 540°C, but the thermocouples are deemed to give accurate within the range of -180°C to 1350°C (TC Ltd. 2004). The thermocouples were cut to the various required lengths and their electrical continuity was tested. Once in place, a temperature trial was carried out whenever possible (embedded thermocouples and those located in the exterior of the building were not tested), in order to test the correct working conditions of the thermocouple-data logger set.

## Internal measurements

One of the fundamental features of the Dalmarnock Fire Tests was to perform “field” measurements of the compartments where the fires took place, in order to generate data for fire modelling validation. A field measurement would consist of placing sensors as densely located as equivalent to model cell resolutions, in order to obtain a detailed characterisation of gas phase properties such as temperature and to some extent velocities (Test One only) and smoke densities. Although the concept of field measurement only applies to the gas phase, solid phase measurements included incident heat fluxes and in-depth temperatures. Since Test One was planned to allow for a full post-flashover fire, “field” type instrumentation was included to measure temperature in the gas phase and

heat flux to surrounding surfaces as well as in-depth temperature measurements and structural monitoring. Nevertheless Test Two was meant as a reference test and was planned to last only for the fire growth period. Therefore gas phase temperatures and heat flux to surroundings were monitored but in-depth temperature measurements and structural monitoring were not applicable.

The ‘gas phase’ temperature measurements were carried out using thermocouples arranged in a series of trees. The thermocouple trees consisted of steel wires fastened both to the ceiling and the floor of the compartment onto which the thermocouple wires were attached using garden wire. 20 of these arrays were installed in each experimental compartment, with 12 thermocouples attached to each. The thermocouples were placed at distances of 0, 50, 100, 200, 300, 400, 600, 800, 1000, 1300, 1600 and 2000 mm from the compartment ceiling. The thermocouple trees were evenly distributed throughout the compartment such that they were not in contact with any solid objects, with the exception of the uppermost thermocouples in each tree which were in contact with the ceiling. It should also be noted that in Test Two one tree (Tree 9, *cf.* Figure 4) had to be taken down and lain on the floor across the front of the sofa just prior to the test and Trees 12 and 15 are in slightly different locations to those in Test One to allow for greater manoeuvrability for the camera crew (*cf.* Figures 3 and 4). A table of coordinates for X,Y locations of thermocouple trees in both tests is presented in annex Tables A1 and A2.

Additionally, 5 trees of 6 thermocouples each were mounted along the window in both tests. The temperature sensors were evenly spaced along the height of the window (at 200 mm height intervals). The thermocouple trees were placed at 400 mm spacing, with one at the centre of the window arrangement. The window sill thermocouple coordinates are presented in annex Table A3 and Figure 7 provides a general overview of all thermocouple tree locations.

A simple laser smoke obscuration sensor was used to measure light attenuation during the fire. It consisted of a small 670 nm Budget 5 Head laser pointer which is placed at some distance from an inexpensive 548 – 716 Centronic photodiode (430-900nm band). Both instruments are mounted in wooden supports. The laser beam is aimed at the photodiode, which generates an output voltage. A 670 nm FB670-10 Narrowband Laser Light filter was fitted on the photodiode wooden support, in order to cut out wavelengths outwith the band emitted by the laser. As the smoke grows denser, the photodiode output signal decreases and calibration of the intensity of this signal against initial intensity provides a correlation can be obtained between the level of obscuration and the output voltage. In turn, this enabled calculation of the local extinction coefficient as per the method outlined in the ‘Error Estimation’ section below. It is important to note that the value of the extinction factor corresponds to an integration of the local absorption coefficient along the entire path length of the laser beam, assuming that scattering is negligible (Fuentes *et al.* 2005).

The laser sensors were calibrated at the University of Edinburgh by measuring the relationship between the incident light power and the output voltage. A laser emitter was

set up at a distance of 300 mm (equal to path length of horizontally aligned laser sensors used in the tests) from a photocell reading incident power. In the laboratory calibration, a polarizer was placed flush with the laser emitter and the intensity of the power incident on the photocell was varied using the polarizer. The photocell was then substituted for a photodiode attached to a voltmeter and the polarizer angle was varied as before, providing a voltage equivalent to every polarizer angle, in turn equivalent to an incident power. This calibration was held in darkness such that only the laser was impinging on the photodiode and photocell. The path length was then increased to 2400mm (as per separation of vertically aligned laser sensors used in the tests) and the full laser beam was still fully impinging on the receiver (low dispersion) such that the power incident *vs.* voltage output correlations was valid in both cases.

Eight of these laser smoke obscuration sensors were placed in each experimental compartment. Five were horizontally aligned (*i.e.* the laser beam was horizontal), attached to the wall separating the living room from Bedroom 1 at a fixed distance  $X$  from the origin. In Test One these were placed at distances of 100, 300, 500, 1000 and 2000 mm from the ceiling, whereas in Test Two they were less spaced at distances of 150, 350, 550, 850 and 1350 mm from the ceiling (*cf.* Figures 3, 4 and 7a). In this case the path length was 300 mm. The remaining three laser sensors were vertically oriented such that the beam spanned most of the height of the room, at 2400 mm (Figure 7d). They were placed approximately along the centreline of the compartment, in the E-W direction, as per Figures 3 and 4. Coordinates for these sensors in Tests One and Two can be found in annex Table A4.

In Test One, Bi-directional Air Velocity Probes were used to characterise the velocities in all openings to the main compartment, *i.e.* through the two internal doorways (the one leading to the kitchen and the one leading to the corridor) and the double-pane window. Air velocities were required to estimate the amount of inflowing and out-flowing air, which in turn allows for an estimation of the heat release rate of the fire. The probes used were conventional bidirectional probes (McCaffrey & Heskestad 1976; Welch *et al.* 2007) with pressure differences logged onto the data loggers using pressure transducers, housed both in the sealed off bathroom and in the 5<sup>th</sup> floor compartment above, where temperatures were expected to remain close to ambient. A total of eight gauges were located in the window opening (3 in front of the NW pane and 5 in front of the SW pane), and three in each of the experimental compartment doorways (*cf.* Figure 7e). Their exact locations are given in annex Table A5. No velocities were measured in the second test. No velocity probes were used in Test Two.

The incident heat flux on a structure is a very important value in terms of fire modelling and fire safety design. A set of thin-skin calorimeters was constructed at the University of Edinburgh, conforming to ASTM E459 (ASTM 2005). They were made of thin copper discs with known thickness and thermophysical properties into which a thermocouple bead was fixed. The copper discs had a diameter of 20 mm and a thickness 2 mm. The device was tightly fitted into a flat bottomed hole of equal dimensions in plasterboard (except when embedded directly in PMMA slab) such that the exposed face was flush with the plasterboard surface. The thermocouple wire came out through the rear of the

wall through a 3 mm diameter hole. When subjected to an external heat flux, there will be a temperature rise on the discs, according to Eq. (1):

$$\dot{q}_{net}'' = \rho c e \frac{\partial T}{\partial t} \quad (1)$$

Where

$\dot{q}_{net}''$  : net heat flux on the disc [energy·time<sup>-1</sup>·area<sup>-1</sup>]

$\rho$  : density [mass·volume<sup>-1</sup>]

$c$  : specific heat [energy·mass<sup>-1</sup>·temperature<sup>-1</sup>]

$e$  : thickness of the disc [length]

$T$  : temperature [temperature]

$t$  : time [time]

Following the equation above, one can conclude that if the change in temperature over time is measured, the net heat flux can be calculated. If the heat losses from the disc are quantified (they include losses by radiation and convection to the surroundings and by conduction to the solid where the sensor is embedded), then the incident heat flux can be estimated. This principle is only valid when the rate of change of temperature over time is non zero, that is, only during transient heating or cooling (this in turn means that the method will cease to be applicable when the disc temperature becomes similar to the surroundings temperature). It is stressed that this is only an approximate measurement, because in order to quantify the heat losses the gas velocity field next to the disc and the temperature of the surroundings must be estimated. Also, the evolution in temperature of the disc thermophysical properties (surface emissivity/absorptivity, specific heat, density) must be known. The energy losses to the backing material were calibrated experimentally and are expressed as a function of the temperature of the disc (Amundarain 2007).

Nine of these thin-skin calorimeters were placed on the ceiling of each experimental compartment, as per Figures 3, 4 and 7c, the coordinates of which are given in annex Table A6. 20 additional heat flux gauges were also mounted on the lightweight steel framing kitchen partition wall on the 4<sup>th</sup> floor in Test One. Refer to annex Figure A1, Figures 7c-7e and annex Table A7 for their location. A 3 by 3 grid of nine heat flux gauges was mounted on the equivalent wall in Test Two, as per the coordinates shown in annex Table A8.

The lightweight steel framing wall was also fitted with thermocouples to measure the in-depth temperature distribution (*cf.* annex Figure A1). The thermocouples placed on the exposed surface (actually, the depth of the thermocouples was 4 mm, but for all practical

purposes they are considered to be on the surface; *cf.* annex Table A9) were embedded in the render of the wall during the building process. Those thermocouples located in the interior of the wall were fixed to the steel stud members using silver soldering. Finally, the thermocouples positioned on the unexposed surface (*i.e.* the kitchen side of the wall) were taped to the plasterboard using insulation tape (Amundarain 2007).

Network cameras were used as imaging devices to provide a visual description of the fire growth. They captured and sent live video to a computer over a Local Area Network. In both tests six cameras were placed in the experimental compartment (*cf.* Figures 3 and 4), while one was used to monitor the Flat Corridor and another the main access corridor outside the flat front door. In Test One, three additional web-cameras were fixed to the external side of the building, at different levels, in order to monitor the fire post-flashover fire expected to develop outside the Test One flat window. These provided several different views allowing for thorough and continuous monitoring of the fire development in both tests. Additional CCTV cameras were installed and footage recorded separately by Xtralis as detailed in Chapter 5.

In order to maximise the recording time, cameras were insulated in order to increase their resistance to the high temperatures expected to develop in the respective compartments. They were wrapped in mineral wool and then covered with aluminium foil. Two cameras were placed at floor height in two holes drilled through the adjoining wall with Bedroom 1. In Test One these were protected behind a fire rated glass (*cf.* Figure 7a) in order to increase their functional longevity throughout the main period of the experiment.

A PMMA slab was installed in the first test as part of ongoing research into sensor driven predictions of flame spread. A slab of PMMA 1000 mm x 300 mm x 25 mm was mounted on a backing sheet of plasterboard using furnace cement. It was screwed onto the wall separating the main compartment from Bedroom 1, about 750mm off the floor, as seen in Figure 7a. The slab contained 23 thermocouples to measure subsurface temperatures and four thin-skin calorimeter heat flux gauges, identical to those described previously, to measure the incident flux on the exposed surface. The positioning of these sensors can be seen in the annex, Figure A2. The thermocouples were embedded from the rear of the sample to within 1mm of the exposed surface of the slab. The heat flux gauges were fitted directly into the PMMA rather than into the plasterboard. The calibration of heat losses from the discs to the PMMA backing was carried out in the laboratory at The University of Edinburgh, following the same process as described above.





Figure 7. Test One experimental compartment photographs looking towards: a) Bedroom 1 (South), b) the window and NW corner, c) the kitchen partition wall (E), d) the heavily fuel-loaded corner (NE), and e) the kitchen doorway (SE).

## External measurements

In multi-storey building fires, vertical fire spread from one floor to other floors is regarded as a serious problem. External flames and the high temperature smoke plume can cause window breakage on floors in the vicinity of the fire, and can even ignite combustible material within upper compartments. Following the same motivation as in the internal measurements, a set of sensors were placed externally in order to provide data as detailed as possible for comparison with computational models. Since it was undesirable for either flames or smoke re-entry to occur in to the room located above the experimental compartment (even though all combustible materials had been removed from the room and therefore the possibility of fire spread had been minimised), the windows of the room were covered with plasterboard, secured to the window frame with screws. This ensured prolonged functionality of the structural sensors located in the 5<sup>th</sup> floor compartment above the fire as well as the pressure transducers used as part of the external air velocity probe measurements afore mentioned. The external measurements were only conducted in Test One.

A total of 152 thermocouples were placed on 19 trees, fixed at seven different X,Y locations along the width of the window and in rows coming out of the window, extending vertically from circa 2/3 of the height of the 4<sup>th</sup> floor window to the top of the 5<sup>th</sup> floor window above (*cf.* Figure 3). Each tree included 8 thermocouples, placed at increasing spacing of 100, 200, 300, 400, 500, 600 and 700 mm above an initial height of 1880mm (Z-coordinate), relative to the global origin. Refer to annex Table A10 for a detailed account of the thermocouple positions.

20 Heat Flux gauges were placed on the external building façade, above the 4<sup>th</sup> floor window. The thermocouple wires for the heat flux gauges were then taken through the window and into the room above the fire compartment and through to the data loggers. 12 of these Heat Flux gauges were placed between the top of the 4<sup>th</sup> floor window and the 5<sup>th</sup> floor window, following the window centreline. They were mounted on the plasterboard covering the 5<sup>th</sup> floor window and on an extra plasterboard section fixed on a steel frame spanning between both windows. The other 8 gauges were mounted on small plasterboard squares and placed along two horizontal lines, 4 along the centre of the 5<sup>th</sup> floor window and 4 immediately above the 4<sup>th</sup> floor window. In order to protect the thermocouple wires from the latter set of gauges - expected to be exposed to the highest temperatures - rock-wool insulation and aluminium foil was wrapped along the exposed spans. Their coordinates are shown in annex Table A11.

Additional external instrumentation includes the eight velocity probes and three external cameras previously described. Three meter rulers, painted in alternate 100mm strips of red and white were placed perpendicular to the façade outside the 4<sup>th</sup> floor window, to be used in conjunction with camera footage to estimate spill plume geometries, should an external fire develop.

## Structural tests

The structural monitoring and tests were only carried out during Test One. The aim of these tests was to obtain data on the behaviour of a full-scale concrete structure when subjected to a realistic and thoroughly monitored compartment fire, which was unprecedented. Also, the performance in fire of two types of FRP strengthening was assessed, in the form of plates and rods. Key aspects of the structural tests included the following:

- The fire load was “real”, resulting from living room/office furniture being burnt rather than from burning wooden cribs, pool fires or gas;
- The structure was a complete building rather than a structural element or set of elements;
- Data relating to the structural behaviour was recorded during both the heating and cooling phases of the fire.

Deflection gauges were used to monitor the floor slab in the 5<sup>th</sup> floor room above the experimental compartment and the partition wall to Bedroom 1. Strain gauges were also used to monitor the upper surface of the ceiling and thermocouples were embedded within the floor slab to monitor temperature of the concrete.

Deflection measurements were taken with Linear Variable Displacement Transducers (LVDT). To monitor the ceiling deflections of the fire compartment an array of 9 transducers were mounted on scaffold bars in the room above the experimental compartment. The scaffold bars were supported on the edge of the floor slab in this room and so the deflections recorded are changes relative to the edge of the slab; any global change in the height of floor was not captured. Using a similar method, horizontal deflections of the internal structural wall of the fire compartment were monitored by three transducers located in Bedroom 1 (*cf.* Figure 1). It is expected that as the room fills with hot gases, the recordings from these transducers will not be entirely reliable due to error induced from rise in ambient temperature. The sensor coordinates for these structural monitoring sensors are given in the annex, Tables A12 and A13.

Slab temperature measurements were taken by means of thermocouples at six different locations in the floor slab above the experimental compartment. At each location temperatures were recorded at four depths within the slab. The thermocouples were inserted in to the slab by drilling an 18mm diameter hole through its entire depth, inserting the thermocouples and then filling the remaining space with cementitious grout. Care was taken to ensure that a small layer of grout was present between the lowest thermocouple and fire compartment so that the temperature measurements were those of the slab and not the hot gases. These thermocouple positions appear in annex Table A14.

Strain measurements were taken at 22 locations on the upper surface of the floor slab above the experimental compartment. Strains were recorded by resistance strain gauges and the results later corrected for temperature variations using the manufacturer's

correction curves. Temperatures were estimated from the nearest thermocouple to each of the strain gauges. The location of the strain gauges is presented in annex Table A15.

Thermocouples and strain gauges were also installed in the FRP plates and rod arrangements described under the 'Additional Demonstrations Non-related to Fire Development' section, above. Their positions are shown in annex Tables A16 and A17, respectively.

### Data Acquisition System

Four data loggers were used during the tests. These were Agilent 34980A units, which can be fitted with up to 8 modules, where the sensors are connected. The majority of the sensors were connected to 40-channel 34921A modules, with built-in reference temperature. About half of the strain gauges were connected to a 34923A module, while the rest were connected to a 34921A board. In the case of the first test, all four data loggers were used: two were located in a room adjacent to the kitchen on the 4<sup>th</sup> floor and were logging the data of the sensors located in the experimental compartment at frequencies of 0.3 Hz and 0.7 Hz; the remaining two were located on the 5<sup>th</sup> floor and were logging data from the external sensors and all the structural sensors, including the deflection gauges located on the 4<sup>th</sup> floor (*cf.* 'Structural tests' section). The main data logger was recording data at a frequency of 0.7 Hz and the second was recording strain gauge data at a frequency of 0.003 Hz. During the second test only two data loggers were used due to the reduced number of sensors. They were both located on the 2<sup>nd</sup> floor, in a room adjacent to the kitchen, logging at frequencies of 0.5 Hz and 0.7 Hz. All data logger data was streamed *live* to a central control room located in a van outside the building. A separate camera hub in Bedroom 1, insulated with rock wool, was used to transferring the camera footage *live* to computers in the external control room where the footage was recorded.

### Error estimation

In conducting large-scale fire tests it is essential to evaluate the potential degree of uncertainty associated to the tests, particularly since it is not always feasible to repeat such tests numerous times.

When the number of observations is too small to justify using the standard deviation to estimate the uncertainty in a measurement, it is usually possible to set limits on the range in which the true value is most likely to lie by carrying out an analysis of the way the values are calculated. An estimation of the uncertainties using error propagation methodology (where applicable) has been conducted, however, these methods are coarse, so the figures presented should only be taken as reference values for the estimated order of magnitude of the uncertainty.

### Potential error associated to the physical phenomena

A comparison between the averaged gas temperature readings of the two tests has been carried out in Chapter 4, comparing both the temperature differences and the time



differences (*cf.* Chapter 4, Figure 6). These results give an idea of the bounds of uncertainty associated not with the measurements and the instruments themselves, but with the uncertainty linked to the fire phenomenon, which could potentially be high due to varying environmental conditions, ventilation parameters, *etc.* So even if there was no uncertainty in the measurements and sensors, there would still be an uncertainty linked to the physical characteristics of the experiment. If an experiment were to be repeated several times, this would not be necessary. Nevertheless, due to the large-scale nature of these experiments multiple repetitions are unfeasible and this comparison is a mechanism to establish a bound of potential errors associated to the general behaviour of the fire.

### **Potential error associated to the measurements**

Beyond the variability of the physical processes there is the error associated to the experimental measurements. It is important to quantify these errors in order to define the degree of uncertainty involved in the actual measurements. This allows for an evaluation of the relevance of the error and influences the conclusions that can be drawn from the data collected.

Two forms of error can be present in the measurements: a magnitude error and a time error. The first error occurs when two sensors that should be reading the same value yield different values and the latter error takes place when two sensors yield the same temperature values but with an associated time delay. Only the first form of error has been estimated here because the second one is not relevant given the timescales of both tests.

Again, rigorously estimating gas-phase measurement errors for these experiments has proved to be a difficult task, since repetition of the experiments for use in statistical analysis is ruled out. The use of analytical expressions to apply error propagation methods will only lead to a lengthy process of which the outcome in terms of comparable accuracy will not justify the resources invested in it. Therefore, a simple error analysis has been conducted providing estimates of the potential errors associated to some of the main instrumentation sensors used.

### **Thermocouple measurement error**

There are three potential sources of error in the recorded thermocouple temperatures. These are instrumentation errors, spatial location errors and radiation errors.

#### ***Instrumentation error***

Sample thermocouple lead was tested at BRE by inserting 60mm of lead into a calibrated temperature block. It was tested as temperatures were increased from ambient up to about 1200°C, the results of which can be seen in Table 1. The error is seen to be notably low throughout, rising at higher temperatures but remaining low relative to the true temperature such that the percentage error remains significantly below 1% all temperatures up to 1000 °C. At 1200 °C the error becomes considerably larger however compartment temperatures are not expected to exceed 1000 °C. During the calibration tests the glass fibre insulation was observed to melt over 1000 °C, however the cable was

tested inside the temperature block, where as in the Dalmarnock experiments the thermocouples are horizontally oriented, so even if the temperature rises about 1000 °C, this should not be a problem. Additionally, these error values correspond only to one sample of thermocouple lead tested and results may differ were more samples to be tested however it provides a good estimate for the order of magnitude of errors expected from instrumentation error.

True Temp. (°C)	Thermocouple lead (°C)	Temp. difference (°C)	Error (%)
99.9	100.0	+0.1	0.10
199.9	199.0	-0.9	0.45
299.9	298.8	-1.1	0.37
400.0	399.1	-0.9	0.23
602.0	605.8	+3.8	0.63
801.8	805.5	+3.7	0.46
1001.2	1002.0	+0.8	0.08
1201.5	1133.6	-67.9	5.65

**Table 1. Respective temperature readings during thermocouple lead calibration tests**

### *Spatial error*

In Tests One and Two, the thermocouple tree were installed by measuring out their distance from the respective global coordinate origin (as per co-ordinates in mm) using two tape meters. Each thermocouple was then attached at a specific height up the tree using a ruler. Hence some degree of error could have been incurred while placing the thermocouples at a given coordinate in space. The significance of these potential errors can be quantified using the dense array of thermocouples to quantify the temperature gradients in space. The potential error per thermocouple location,  $r_{err}$  (mm) is defined as:

$$r_{err} = \sqrt{x_{err}^2 + y_{err}^2 + z_{err}^2} \quad \text{— — — — — (2)}$$

Where  $x_{err}$ ,  $y_{err}$  and  $z_{err}$  are the degree of error in each of the three directions (mm). The local temperature gradient in space is then calculated using the temperature difference between a thermocouple and those at a known distance in its immediate vicinity, such that for each, the gradient is:

$$\frac{dT}{dr} = \frac{(T_2 - T_1)}{\sqrt{dx^2 + dy^2 + dz^2}} \quad (3)$$

Where  $T_n$  are the temperatures in neighbouring thermocouples and  $dx$ ,  $dy$ ,  $dz$  are the potential maximum distances between the respective coordinates of these thermocouples.



Although the instruments used to locate the coordinates had mm markings, the distances measured were large hence it is likely errors could be up to 10 mm in each direction, rendering a potential error of 17.3 mm per thermocouple as per Eq. (2). When using distances between two thermocouples to obtain temperature gradients, the maximum potential error is two fold and hence 34.6 mm.

Thermocouple tree 12 in Test One was chosen for comparison of temperature gradients, as one of the trees represents average distances to neighbouring trees while not in the direct vicinity of heavy fuel loading (*cf.* Figure 3). Test One data was used to calculate temperature gradients for the penultimate thermocouple (at 1600mm) from the ceiling as it has the largest spacing to thermocouples above (300mm) and beneath (400mm) it. Temperature gradients were obtained between this thermocouple and those above and below as well as between thermocouples at an equivalent height in neighbouring Trees 8, 9, 14 and 15 (*cf.* Figure 3), using Eq. (3). The average of each of these gradients throughout the duration of Test One yielded a maximum gradient of 0.39 °C per mm in the horizontal direction and 0.51 °C per mm in the vertical direction, which was larger as expected due to the tendency towards stratification of the buoyant hot products of fire.

Hence, the maximum potential error in thermocouple readings due to spatial error, calculated as the product of the maximum gradient and the maximum potential spatial error, is circa 18 °C. Although greater than the instrumentation error, this is still a relatively low error compared to compartment temperatures in a fire, particularly as it is an upper bound representation of error.

### Radiation error

The third source of error in thermocouple readings is due external factors such as remote radiation influencing the reading. The thermocouple data obtained in the tests is corrected for radiation (excluding thermocouples in touch with solids) according to the methodology described by Welch *et al.* (2007). The potential error is then assumed to be of the same order of magnitude as the correction required. Data from Test One is used for an assessment of potential radiation error in the thermocouple measurements.

Table 2 shows several calculated errors following the aforementioned methodology based on two thermocouple trees which were located at the centre of the experimental compartment. The difference between the raw values and the corrected gas-phase temperatures was calculated for the entire duration of the test, and then was averaged in time. Two heights were chosen for each thermocouple tree, to obtain an idea of the differences between those measurements carried out in the hot layer and those in the cold layer.

Thermocouple Tree	Height (mm)	Uncertainty (%)
8	2400	0.45
8	450	0.36
14	2400	0.8
14	450	0.45

**Table 2. Gas-phase temperature measurement error estimation**

As explained in detail in Welch *et al.* (2007) errors are greater in the cold layer as expected. Again, potential errors remain below 1%. Although errors from only two thermocouple trees have been shown here, and a more pronounced peak correction in temperatures may result elsewhere, they provide a representation of the magnitude of the errors expected due to radiation error throughout the compartment. Additional details of radiation errors corrected for in each test can be found in Chapters 3 and 4.

Overall individual sources of errors in thermocouple measurements appear to be negligible, apart from potential localised peak radiation errors which are corrected for in both tests as detailed in Chapters 3 and 4. An assessment of cumulative error due to all three sources of error has not been conducted as it would only be possible as an estimate of upper bound error which is not thought to be representative of realistic error due to its low probability of occurrence. Hence thermocouple data from the dense array of sensors placed throughout the compartment is deemed to provide an accurate representation of gas-phase temperatures.

### Extinction coefficient

Bouguer's Law as applied to smoke is the basis for relating optical measurement and mass concentration. Specifically, this law relates the ratio of the transmitted ( $I$ ) and initial incident intensities ( $I_0$ ) to the mass concentration extinction coefficient ( $K_{ext}$ ) and the path length through the smoke, ( $L$ ) as per Eq. (4):

$$\frac{I}{I_0} = \exp(-K_{ext}L) \quad (4)$$

The error of  $K_{ext}$  is calculated using Eqs. (5-7) as follows:

$$\frac{dK_{ext}}{K_{ext}} = \frac{d \ln(I_0/I)}{\ln(I_0/I)} + \frac{dL}{L} \quad (5)$$

Where the error in the extinction is defined as

$$d \ln(I_0/I) = \left| \frac{\partial \ln(I_0/I)}{\partial I_0} \right| dI_0 + \left| \frac{\partial \ln(I_0/I)}{\partial I} \right| dI \quad (6)$$

The error in the extinction coefficient is finally obtained by

$$\frac{dK_{ext}}{K_{ext}} = \frac{1}{\ln(I_0/I)} \left( \frac{dI_0}{I_0} + \frac{dI}{I} \right) + \frac{dL}{L} \quad (7)$$

The uncertainties of the initial incident light intensity,  $I_0$ , and the transmitted light intensity,  $I$ , were calculated on a sample of 150 measurements from a laser smoke obscuration receiver taken prior to the start of the tests when monitoring only ambient conditions. Since the data was seen to fluctuate, the true value was taken as the mean value obtained from this data and the associated uncertainty as the standard deviation of

this mean. Values varied within a range of  $\pm 0.3\%$  for  $I_0$  and  $\pm 0.4\%$  for  $I$ . The relative uncertainties in  $K_{ext}$  were calculated for a ratio of  $I_0/I$  varying from 1.1 to 1.4, giving a potential error in the extinction coefficient varying from 2.5 to 10.0% for the pre-flashover period during which the sensors were functional. While this error is only expected to increase as the smoke becomes denser, it provides an upper bound and lower bound range within which the data is deemed to be accurate. These ranges were taken into account in the implementation of the extinction coefficients for thermocouple temperature for radiation errors, and the effect of the bounds was assessed, as detailed in Chapters 3 and 4.

## Heat flux measurement

A similar method was applied in the estimation of the errors associated with heat flux measurements. The incident heat flux is related to the heat losses as indicated in Eq. (8), assuming that the thermal inertia of the copper disc is small enough for the process to be considered as in steady state (these equations were developed following the analysis carried out by Amundarain 2007):

$$\dot{q}_e'' = \frac{1}{(1-C)} [\varepsilon \sigma (T_s^4 - T_0^4) + h(T_s - T_0)] \quad (8)$$

Where,

- $\dot{q}_e''$  : incident (radiative) heat flux on the disc [energy·time<sup>-1</sup>·area<sup>-1</sup>]
- $C$  : fraction of the incident heat flux that is conducted away to the embedding material
- $\varepsilon$  : surface emissivity (assumed equal to the surface absorptivity)
- $\sigma$  : Stefan-Boltzmann constant [energy·time<sup>-1</sup>·area<sup>-1</sup>·temperature<sup>-4</sup>]
- $T_s$  : surface temperature [temperature]
- $T_0$  : overall surroundings temperature [temperature]
- $h$  : convective coefficient [energy·time<sup>-1</sup>·area<sup>-1</sup>·temperature<sup>-1</sup>]

And its error can be defined as,

$$d\dot{q}_e'' = \left| \frac{\partial \dot{q}_e''}{\partial C} \right| dC + \left| \frac{\partial \dot{q}_e''}{\partial T_s} \right| dT_s + \left| \frac{\partial \dot{q}_e''}{\partial T_0} \right| dT_0 \quad (9)$$

Or expressed as a ratio to the true value and after some simplification,

$$\frac{d\dot{q}_e''}{\dot{q}_e''} = \frac{d(1-C)}{(1-C)} + \left| \frac{4\varepsilon \sigma T_s^3 + h}{\varepsilon \sigma (T_s^4 - T_0^4) + h(T_s - T_0)} \right| T_s \frac{dT_s}{T_s} + \left| \frac{-4\varepsilon \sigma T_0^3 - h}{\varepsilon \sigma (T_s^4 - T_0^4) + h(T_s - T_0)} \right| T_0 \frac{dT_0}{T_0} \quad (10)$$

The Eq. (10) expression shows that the error will depend on the temperature difference between the copper disc and the surroundings. For a 250°C difference between the disc and the surroundings, the calculated error is of 10.0%, while for a 50°C difference the error mounts up to 158.9% (the extreme case is for equal temperatures, where the solution diverges). This is due to the principle of operation of this type of heat flux, described in the 'Internal measurements' section. The individual uncertainties used were 1.2% for  $C$  (Amundarain 2007), 8.8% for  $T_s$  (Reszka 2007), and 0.8% for  $T_0$ , as per the maximum error associated to the representative gas-phase temperature correction for radiation, as detailed in the 'radiation error' section above.

## Summary

An error analysis has been conducted for the measurements undertaken in both tests while potential sources of error associated to other sensors, used only in Test One, are discussed in the relevant chapters. The analysis shows that errors associated to measurement techniques are small when compared to the potential variability of a complex experiment that was only conducted twice. Therefore this remains the largest potential source of error and will be discussed further in Chapter 4 when comparing the results of both tests.

## References

- Amundarain (2007), Assessment of the Thermal Efficiency, Structure and Fire Resistance of Lightweight Building Systems for Optimised Design, PhD Thesis, Uni. Edinburgh.
- ASTM (2005) ASTM E459 - 05: Standard Test Method for Measuring Heat Transfer Rate Using a Thin-Skin Calorimeter.
- British Standards (1993), Fire Tests on Building Materials and Structures, BSI, U.K., BS476: Part 33: 1993 (ISO 9705:1993).
- Fuentes, A., Legros, G., Joulain, P., Vantelon, J.P., Torero, J.L. (2005), Evaluation of the Extinction Factor in a Laminar Flame Established over a PMMA Plate in Microgravity, *Microgravity Sci. Technol.*, 17, 10-14.
- McCaffrey, B.J. & Heskestad G. (1976), A Robust Bidirectional Low-Velocity Probe for Flame and Fire Application, *Combustion and Flame* 26, 125-127.
- Reszka, P., Torero, J.L. (2007), In-Depth Temperature Measurements in Wood Exposed to Intense Radiant Energy, 5<sup>th</sup> Med. Combustion Symposium, Tunisia.
- TC Ltd. (2004), TC Guide to Thermocouple and Resistance Thermometry, Issue 6.0, UK.
- Tewarson, A. (1995), Generation of Heat and Chemical Compounds in Fires, in *SFPE Handbook of Fire Protection Engineering*, 2nd Edition, Edited by DiNenno *et al.* NFPA, USA.
- Welch, S., Jowsey, A., Deeny, S., Morgan, R. & Torero, J.L., (2007), BRE large compartment fire test – characterising post flashover fires for model validation, *Fire Safety Journal*, in press.

## Annex. Instrument locations

This annex contains detailed tables of coordinates for most sensor locations, relative to the respective global coordinate origins for Test One and Test Two. In places, diagrams provide additional information on dimensions and visualisation of sensor distribution.

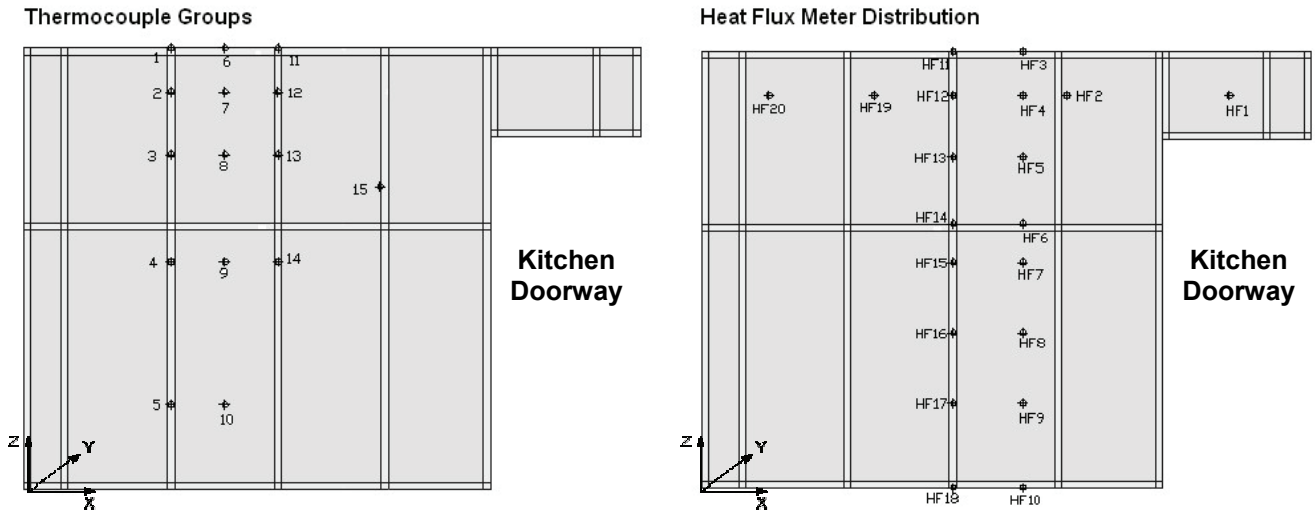


**Figure A1. Test One: Lightweight steel framing wall sensor locations relative to a local coordinate system as labelled (extracted from Amundarain, 2007).**

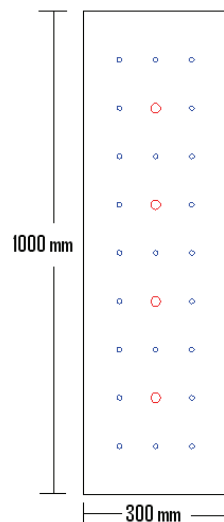


**Figure A2. Test One: Positioning of sensors in PMMA slab. Small blue circles represent thermocouples, while larger red circles represent thin-skin calorimeter heat flux gauges.**

X (mm)	Y (mm)	Thermocouple Tree
4230	3160	1
4250	2060	2
4195	1315	3
4615	190	4
3605	2955	5
3660	1220	6
2860	3325	7
2590	1945	8
3025	350	9
2270	3160	10
2115	2580	11
2305	1030	12
1605	3150	13
1765	1900	14
1910	330	15
510	2815	16
750	2025	17
360	1515	18
390	710	19
800	350	20

**Table A1. Test One: thermocouple tree coordinates in the main compartment (cf. Figure 3).**

X (mm)	Y (mm)	Thermocouple Tree
4230	3160	1
4250	2060	2
4195	1315	3
4615	190	4
3605	2955	5
3660	1220	6
2860	3325	7
2590	1945	8
2270	3160	10
2115	2580	11
2610	1155	12
1605	3150	13
1765	1900	14
1760	1020	15
510	2815	16
750	2025	17
360	1515	18
390	710	19
800	350	20

**Table A2. Test Two: thermocouple tree coordinates in the main compartment (cf. Figure 4).**



Thermocouple Tree Coordinates		Thermocouple Heights per Tree
X (mm)	Y (mm)	Z (mm)
-5	720	2150
-5	1120	1950
-5	1520	1750
-5	1920	1550
-5	2320	1350
		1150

**Table A3. Tests One and Two: Window sill thermocouple coordinates.**

Test One			Test Two		
X (mm)	Y (mm)	Z (mm)	X (mm)	Y (mm)	Z (mm)
3300	0	2350	3400	0	2300
3300	0	2150	3400	0	2100
3300	0	1950	3400	0	1900
3300	0	1450	3400	0	1600
3300	0	450	3400	0	1100
350	2000	25	620	1640	25
2670	1850	25	2800	1640	25
4200	1900	25	4120	1640	25

**Table A4. Tests One and Two laser smoke obscuration receiver coordinates.**

Local Name	Global Coordinates		
	X (mm)	Y (mm)	Z (mm)
Door 1 - Top	4270	-680	1810
Door 1 - Mid	4270	-680	1610
Door 1 - Bot	4230	-680	460
Door 2 - Top	4740	400	1890
Door 2 - Mid	4740	400	1750
Door 2 - Bot	4740	400	430
External 1	-300	1350	1390
External 2	-300	1795	1695
External 3	-300	1375	1850
External 4	-300	1685	2095
External 5	-300	1375	2230
External 6	-300	995	1730
External 7	-300	995	2095
External 8	-300	2095	2130

**Table A5. Test One: Bi-directional Air Velocity Probe coordinates for both the doorways and window.**

X (mm)	Y (mm)	Z (mm)
4140	2950	2441
4100	2055	2441
4100	1140	2441
2290	2965	2441
2755	2080	2441
2310	1115	2441
685	2835	2441
995	2025	2441
815	660	2441

**Table A6. Tests One and Two: Ceiling heat flux gauge coordinates.**

Local Name	X (mm)	Z (mm)	Local Name	X (mm)	Z (mm)
HF1	2970	2230	HF11	1445	2480
HF2	2050	2230	HF12	1445	2230
HF3	1745	2480	HF13	1445	1880
HF4	1745	2230	HF14	1445	1500
HF5	1745	1880	HF15	1445	1280
HF6	1745	1500	HF16	1445	880
HF7	1745	1280	HF17	1445	480
HF8	1745	880	HF18	1445	0
HF9	1745	480	HF19	950	2230
HF10	1745	0	HF20	350	2230

**Table A7. Test One: Lightweight steel framing wall heat flux gauge coordinates relative to local origin as indicated in Figure A1.**

X (mm)	Y (mm)	Z (mm)
4650	3100	450
4650	2100	450
4650	1120	450
4650	3100	1450
4650	2100	1450
4650	1120	1450
4650	3100	2150
4650	2100	2150
4650	1120	2150

**Table A8. Test One: Kitchen partition wall heat flux gauge coordinates.**

Local Name	Group	X (mm)	Y (mm)	Z (mm)	Comment	Local Name	Group	X (mm)	Y (mm)	Z (mm)	Comment
TC1	2	1450	54	2230	A	TC21	4	1450	218	1280	E
TC2	2	1450	124	2230	B	TC22	5	1450	4	480	D
TC3	2	1450	194	2230	C	TC23	5	1450	218	480	E
TC4	3	1450	54	1880	A	TC24	6	1750	4	2480	D
TC5	3	1450	124	1880	B	TC25	7	1750	4	2230	D
TC6	3	1450	194	1880	C	TC26	7	1750	124	2230	B
TC7	4	1450	54	1280	A	TC27	7	1750	218	2230	E
TC8	4	1450	124	1280	B	TC28	8	1750	4	1880	D
TC9	4	1450	194	1280	C	TC29	8	1750	124	1880	B
TC10	12	2050	54	2230	A	TC30	8	1750	218	1880	E
TC11	13	2050	54	1880	A	TC31	9	1750	4	1280	D
TC12	14	2050	54	1280	A	TC32	9	1750	218	1280	E
TC13	15	2625	124	1700	B	TC33	10	1750	4	480	D
TC14	5	1450	54	480	A	TC34	10	1750	218	480	E
TC15	1	1450	4	2480	D	TC35	11	2050	4	2480	D
TC16	2	1450	4	2230	D	TC36	12	2050	4	2230	D
TC17	2	1450	218	2230	E	TC37	12	2050	218	2230	E
TC18	3	1450	4	1880	D	TC38	13	2050	4	1880	D
TC19	3	1450	218	1880	E	TC39	13	2050	218	1880	E
TC20	4	1450	4	1280	D	TC40	14	2050	4	1280	D
<b>Comment Key:</b> A=Exposed Flange, B=Flange/Mineral Wool Centre, C=Unexposed flange, D=Exposed Surface, E=Unexposed Surface.											

**Table A9. Test One: Lightweight steel framing wall thermocouple coordinates relative to local origin as indicated in Figure A1.**

X (mm)	Y (mm)	External Thermocouple Tree
-270	30	E1
-270	530	E2
-270	1030	E3
-270	1530	E4
-270	2030	E5
-270	2530	E6
-270	3030	E7
-500	530	E8
-500	1530	E9
-500	2530	E10
-750	530	E11
-750	1530	E12

X (mm)	Y (mm)	External Thermocouple Tree
-750	2530	E13
-1000	530	E14
-1000	1530	E15
-1000	2530	E16
-1250	530	E17
-1250	1530	E18
-1250	2530	E19

**Table A10. Test One: External thermocouple tree coordinates (cf. Figure 3), continued from previous page.**

X (mm)	Y (mm)	Z (mm)
-320	1540	2455
-320	1540	2705
-320	1540	2955
-320	1540	3205
-320	1540	3455
-320	1540	3705
-240	1460	3910
-240	1460	4110
-240	1460	4310
-240	1460	4510
-240	1460	4710
-240	1460	4910
-280	2515	2455
-280	1815	2455
-280	1265	2455
-280	565	2455
-240	2450	4510
-240	1820	4510
-240	1260	4510
-240	630	4510

**Table A11. Test One: External heat flux gauge coordinates.**

X (mm)	Y (mm)	Z (mm)
830	1800	2650
1490	1980	2650
2450	660	2650
2450	1310	2650
2370	1840	2650
2450	2450	2650
2580	3040	2650
3180	1920	2650
3900	1870	2650

**Table A12. Test One: Concrete slab displacement transducer coordinates.**

X (mm)	Y (mm)	Z (mm)
2450	0	1830
2450	0	1220
2450	0	610

**Table A13. Test One: Internal partition wall (to Bedroom 1) displacement transducer coordinates.**

Location on Slab		Thermocouple Height per Location	
X (mm)	Y (mm)	Z (mm)	
190	170	2500	
2000	15	2550	
1900	4650	2600	
1590	1070	2650	
1980	3630		
3500	4530		

**Table A14. Test One: Concrete slab thermocouple coordinates.**

X (mm)	Y (mm)	Z (mm)
2420	3400	2650
2420	2680	2650
2420	2040	2650
2420	925	2650
2420	150	2650
2190	2040	2650
1940	2040	2650
1560	3400	2650
1560	2040	2650
1560	150	2650
1360	2040	2650
1180	3680	2650
1180	3400	2650
1180	2040	2650
1180	925	2650
1180	150	2650
50	2040	2650
2420	2040	2650
1560	2040	2650
1180	2040	2650
50	2040	2650

**Table A15. Test One: Concrete slab strain gauge coordinates.**

X (mm)	Y (mm)	Z (mm)
1180	1290	2500
1180	2040	2500
1180	2790	2500
1360	1290	2500
1360	2040	2500
1360	2790	2500
1560	1290	2500
1560	2790	2500
1560	2790	2500
1940	1290	2500
1940	2040	2500
1940	2790	2500
2190	1290	2500
2190	2040	2500
2190	2790	2500
2420	1290	2500
2420	2040	2500
2420	2790	2500
1890	2040	2500
1915	2040	2500

**Table A16. Test One: FRP thermocouple coordinates.**

X (mm)	Y (mm)	Z (mm)
2420	2790	2500
2420	2040	2500
2420	1290	2500
2190	2790	2500
2190	2040	2500
2190	1290	2500
1940	2790	2500
1940	2040	2500
1940	1290	2500
1560	2790	2500
1560	2040	2500
1560	1290	2500
1360	2790	2500
1360	1290	2500
1180	2790	2500
1180	2040	2500
1180	1290	2500
3180	2040	2650

**Table A17. Test One: FRP strain gauge coordinates.**



The opinions expressed in this volume are those of the named authors of each of the chapters and may not represent the opinions of the editors, the School of Engineering and Electronics or the University of Edinburgh.

When citing chapters from this volume, the following reference style should be used:

Authors, Chapter no., Title, *The Dalmarnock Fire Tests: Experiments and Modelling*, Edited by G. Rein, C. Abecassis Empis and R. Carvel, Published by the School of Engineering and Electronics, University of Edinburgh, 2007. ISBN 978-0-9557497-0-4

The contents of this book and much of the other published output from the BRE Centre for Fire Safety Engineering can be downloaded from the Edinburgh Research Archive:

**<http://www.era.lib.ed.ac.uk/handle/1842/1152>**

**Produced as part of the FIRESEAT symposium series:**

**<http://www.see.ed.ac.uk/FIRESEAT/>**

Published by the

**SCHOOL *of* ENGINEERING *and* ELECTRONICS  
UNIVERSITY *of* EDINBURGH**

**KING'S BUILDINGS, MAYFIELD ROAD  
EDINBURGH, EH9 3JL, UNITED KINGDOM**

**Tel: +44 (0) 131 650 1000**

**Fax: +44 (0) 131 650 6554**

**[fire.research@ed.ac.uk](mailto:fire.research@ed.ac.uk)**

**<http://www.see.ed.ac.uk/fire/>**

November 2007

**Copyright © the School of Engineering and Electronics, University of Edinburgh**